pp. 86–91.
[24]T. Nagamiya, K. Yosida, and R. Kubo, Advan. Phys. 4, 2 (1955).
[25]M. E. Fisher, Proc. Roy. Soc. (London), A254, 66 (1960).
[26]A. Bienenstock, J. Appl. Phys. 37, 1459 (1966).

PHYSICAL REVIEW B VOLUME 2, NUMBER 5 1 SEPTEMBER 1970

Neutron and Optical Investigation of Magnons and Magnon-Magnon Interaction Effects in NiF_2

M. T. Hutchings* and M. F. Thorpe*
Brookhaven National Laboratory, Upton, New York 11973
and
R. J. Birgeneau,† P. A. Fleury, and H. J. Guggenheim
Bell Telephone Laboratories, Murray Hill, New Jersey 07974
(Received 7 April 1970)

Neutron inelastic scattering and Raman light scattering have been used to investigate spin-wave excitations in the canted antiferromagnet NiF_2. All the zone-center Raman-active phonons have been observed as well. By neutron scattering, we have measured the dispersion of one-magnon excitations in the (010) plane of the crystal. These data have been analyzed, together with published values for the antiferromagnetic-resonance mode frequencies, to give values for the two anisotropy parameters and three exchange constants in the spin Hamiltonian for the crystal. We find $D=4.36\ (\pm 0.14)\ cm^{-1}$, $E=1.66\ (\pm 0.03)\ cm^{-1}$, J_1 (coupling ions along the c axis) $=-0.22\ (\pm 0.50)\ cm^{-1}$, J_2 (coupling corner to body center ions) $=13.87\ (\pm 0.36)\ cm^{-1}$, and J_3 (coupling ions along the a or b axes) $=0.79\ (\pm 0.40)\ cm^{-1}$. From these parameters, we have calculated the density of magnon states and find that it shows one sharp peak near 108 cm^{-1}. The one-magnon Raman scattering confirms the values of the antiferromagnetic-resonance frequencies, while the second-order (two-magnon) scattering gives a broad line corresponding to a weighted two-magnon density of states centered at 203 cm^{-1}. We have interpreted the two-magnon line shape in terms of the neutron data by a Green's-function theory which includes the effect of magnon-magnon interaction. In this theory of line shape, the density of states is approximated by a one-exchange-parameter model, corresponding to a weighted zone-boundary energy. Nevertheless, excellent agreement with experiments is obtained. This study, therefore, has served to characterize completely the interactions in NiF_2, and, in addition, it has supplied the first detailed comparison of neutron and Raman data for an $S=1$ ion.

I. INTRODUCTION

Nickel fluoride NiF_2 has the rutile crystal structure[1] and orders below 73.2 °K[2] to form a slightly canted two-sublattice antiferromagnet. Unlike the isomorphic compounds MnF_2, FeF_2, and CoF_2, the spins lie in the a-b plane of the crystal and are tilted away from the axes by a small angle $\sim 0.5°$.[3–5] This tilt gives rise to a small ferromagnetic moment which modifies the magnetic properties from those of a conventional antiferromagnet.[6–8]

We have investigated the magnon dispersion relations in this compound by both neutron scattering and light scattering. By inelastic neutron scattering, the dispersion may be studied throughout the Brillouin zone, since the neutron wave vector is of the same order of magnitude as that of the shortest-wavelength magnons. The data may be readily analyzed to obtain values for the anisotropy and exchange constants in the spin Hamiltonian of the crystal. Indeed, neutron scattering is perhaps the most direct method of obtaining exchange constants in an antiferromagnetic compound. In the case of NiF_2, it permits unambiguous determination of the values whereas other methods have previously given conflicting results.[6–10]

Raman light scattering provides information on both one- and two-magnon excitations, as well as optical phonons. However, the technique is limited to exploration of small wave-vector excitations because of the small momentum carried by the incident photons $\approx 10^{-3}$ Å^{-1}. In first-order scattering, therefore, Raman experiments provide information only on the excitations near the center of the Brillouin zone. This is true for both one-magnon and phonon excitations. However, light scattering is also sensitive to two-magnon excitations of essen-

tially zero total wave vectors. These excitations are formed of pairs of magnons having equal and opposite wave vectors whose individual wave vectors range throughout the Brillouin zone. The results of these second-order light scattering experiments may then be compared with the results found from neutron scattering. In particular, as we shall see, the two-magnon excitation observed in the optical experiments is not the simple sum of two individual magnons, but that magnon-magnon interaction effects are observable and significant. Such effects have been calculated and observed in $RbMnF_3$,[11,12] a cubic antiferromagnet, and in MnF_2[13] and FeF_2,[14] which have the rutile structure. In the present case we compare the neutron and Raman data for an $S=1$ ion for the first time.[15]

In Sec. II we shall describe the crystal and magnetic structure in detail as well as the method of crystal preparation. In Sec. III we discuss the theory of spin waves in NiF_2, and in Sec. IV we describe the neutron scattering measurements and their results. The Raman light scattering is described in Sec. V, and the theory of the line shape is given in Sec. VI, where the neutron and light scattering results are compared. The results are summarized in Sec. VII.

II. CRYSTAL STRUCTURE AND SAMPLE PREPARATION

The rutile crystal structure of NiF_2 is shown in Fig. 1. The space group in the paramagnetic state is $D_{4h}^{14}-P4/mnm$, and the point symmetry of the Ni^{2+} ion site is D_{2h}. The arrangement of the F^- ions around the Ni^{2+} sites may be considered to be distorted octahedra. At 25 °C the lattice parameters are $a_0=4.6506$ Å, $c_0=3.0836$ Å, and $u=0.310$.[1] Below the Néel temperature magnetostriction causes the symmetry to change to orthorhombic; however, this distortion is very small and may be neglected for our purposes. The average lattice constants at 21.4 °K are $a_0=4.6474$ Å and $c_0=3.0750$ Å.[16]

Single-crystal NiF_2 was grown from the melt using a modification of Stockbarger's method. NiF_2 is reported to have a vapor pressure of 1 atm at about 1000 °C and a melting point over 1300 °C. For these reasons it is impractical to grow from the melt using conventional methods, but a sealed platinum container has been found to overcome the difficulties. Dry NiF_2 was prepared by passing HF over "low cobalt" $NiCl_2$ at 850 °C for 16 h. The resulting material was a light greenish-yellow. The material was loaded into a Pt–10% Rh alloy tube and then lowered through a hot zone (1420 °C) at 1 mm per hour. After 100 h the tube was removed at room temperature and opened by cutting along the length with a circular diamond saw. The NiF_2 boule was emerald green, weighing 56 g, and was

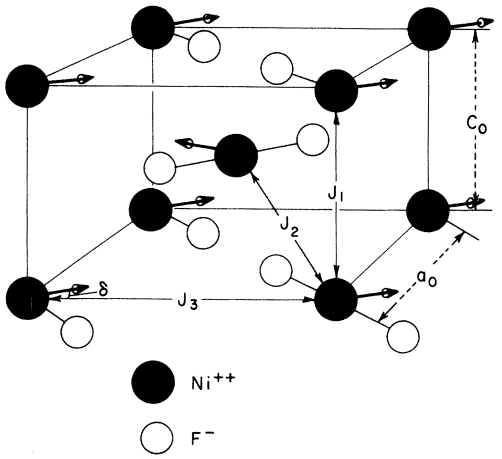

FIG. 1. Crystal structure and magnetic structure of NiF_2. The canting angle δ is exaggerated in the diagram for clarity. The first three neighbor interaction constants are indicated.

2 in. long and $\frac{3}{4}$ in. in diam. Although there were many cracks, there were clear areas as large as a $\frac{1}{2}$-in. cube which were shown to be nearly single crystals. From the clear area, two samples, both approximately 0.5 cc in volume, were cut.

Both samples were single crystals but with rather large mosaic spreads and, in particular, when used for the neutron scattering had a mosaic spread of ~ 1.5 – 2.0° full width at half-maximum (fwhm). Nevertheless, in view of the difficulty of sample preparation and the fact that it was the only large sample available, measurements were carried out using it. The large mosaic spread must be borne in mind during the analysis of the results (Sec. IV).

III. THEORY OF MAGNETIC STATE

A. Molecular Field Theory

The theory of the magnetic properties of NiF_2 has been discussed by Moriya,[6,17] and the symmetry properties have been discussed by Joshua and Cracknell.[18] The energy levels of the Ni^{2+} ion are shown in Fig. 2. The properties of the ground-orbital singlet state may be described by the spin Hamiltonian

$$\mathcal{H}^{(p)} = DS_{z''}^{(p)2} \pm E(S_{x''}^{(p)2} - S_{y''}^{(p)2}) \ , \qquad (1)$$

where $S=1$. The upper sign in Eq. (1) applies to the corner site ($p=i$), and lower one to the body-center site ($p=j$), the z'' axis here is along the crystal c axis, and x'' and y'' are at 45° to the crystal a and b axes. Peter and Mock[19] have measured the spin-Hamiltonian parameters for Ni^{2+} in the isomorphic lattice ZnF_2 and find $g=2.33$, $D=4.19$ cm^{-1}, and $E=2.67$ cm^{-1}.

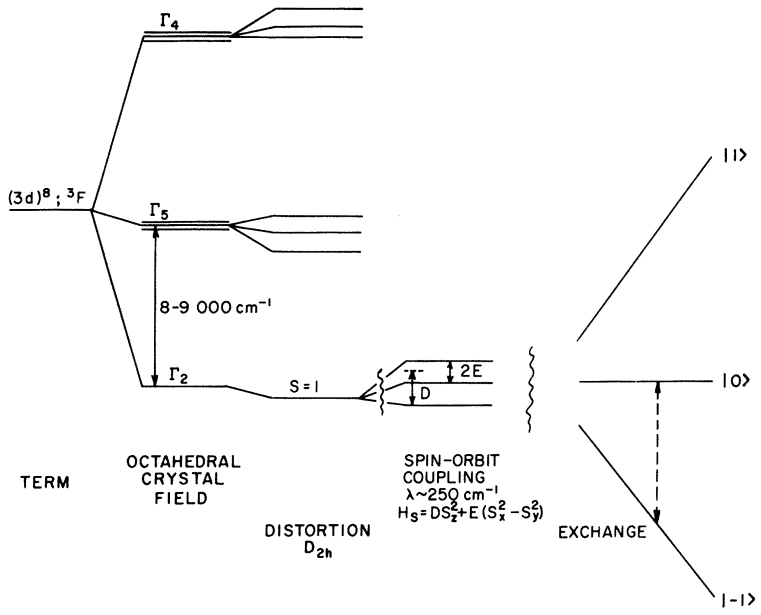

FIG. 2. Energy levels of NiF_2, showing the splitting of the $(3d)^8$, ^3F, term under the orthorhombic crystal field, spin-orbit coupling, and exchange field.

In the rutile structure it is usually found that the exchange interaction, which we write in the Heisenberg form, is appreciable between at least three types of neighbors. These are indicated in Fig. 1. We write the spin Hamiltonian for the crystal as

$$\mathcal{H}=\sum_i \mathcal{H}_s^i+\sum_j \mathcal{H}_s^j+\sum_l \sum_{\langle m-\delta_l\rangle} J_l \vec{S}_m\cdot\vec{S}_{m+\delta_l}+\mathcal{H}_{dd}\,, \quad (2)$$

where l is summed over the different types of neighbor, and $\langle m-\delta_l\rangle$ denotes the sum over all pairs of the lth neighbor ions m and $m+\delta_l$, each pair being included only once. The fourth term represents the dipolar interaction. This is a small term and in the present work we neglect its dispersion and include it in the effective value of D. We also include in D any anisotropic exchange present, although this is expected to be small. The effect of antisymmetric exchange, which may be present between individual pairs of next-nearest-neighbor ions, averages to zero on summation in the molecular field approximation.

Molecular field theory may be used to determine the antiferromagnetic ground state. The positive axial single-ion anistropy D causes the spins to lie in the a-b plane where competition between the rhombic term E, which tends to align the spins at 90°, and exchange, which tends to align them antiparallelly, causes a canting of the spins in this plane. The canting angle δ between the spins and the a axis is easily seen to be $|\delta|=E/8J_2$. We shall see that this relation is slightly modified by spin-wave theory. The δ has been estimated by a number of authors to lie between 0.38 and 2.5°.[5,8,10] Thus the spin structure, shown in Fig. 1, may give rise to four types of domains corresponding to the possible directions of the ferromagnetic moment.

Several authors[10,20,21] have discussed the antiferromagnetic resonance modes in NiF_2 and shown that there are two modes with different energies. The upper mode corresponds to the precession of the spin vector predominantly out of the a-b plane against the anisotropy parameter D, while the lower mode in the a-b plane precesses against the anisotropy parameter E. The former is antiferromagneticlike whereas the latter is more ferromagnetic in nature. The physical picture of these modes is important in the discussion of the spin-wave theory below.

B. Spin-Wave Theory

The transformation of the Hamiltonian Eq. (2) to spin-wave variables and the determination of the energy dispersion relations is fairly straightforward except for the single-ion anisotropy terms which we now discuss.

1. *Single-Ion Anisotropy Terms*

It has been pointed out by Walker[22] that care must be taken when expressing the single-ion anisotropy spin operators in terms of the first-order spin deviation (boson) operators at each site. If one chooses as one's criterion that the matrix elements of the crystal field operator expressed in boson representation should reproduce those of the original spin operators between corresponding states, then one finds, for example,[22]

$$O_2^0=3S_z^2-S(S+1)\to-6S\eta a^\dagger a+S(2S-1)\,, \quad (3a)$$

where

$$\eta = (1 - 1/2S)$$

and

$$O_2^2 = S_x^2 - S_y^2 \rightarrow S\eta'(a^\dagger a^\dagger + aa) \quad , \tag{3b}$$

where

$$\eta' = (1 - 1/2S)^{1/2} \quad .$$

The above operator for O_2^0, Eq. (3a), reproduces the diagonal matrix elements for $S_z = S$ and $S_z = S - 1$ but not $S_z = S - 2$. Similarly, (3b) reproduces the matrix element $\langle S-2| \, |S\rangle$ correctly but not $\langle S-3| \, |S-1\rangle$. Walker has emphasized, therefore, that the above prescription is probably not foolproof.

If we derive the energies for the antiferromagnetic resonance modes in NiF_2 using (3a) and (3b), we find

$$E_0(1) = (32J_2\eta D + 4\eta'^2E^2)^{1/2} \quad , \tag{4a}$$

$$E_0(2) = [(\eta^2 - \eta'^2)D^2 + 16J_2D(\eta - \eta') + 4\eta(\eta' + 3\eta)E^2]^{1/2} \tag{4b}$$

However, as Richards has discussed, the lower mode with energy $E_0(2)$ corresponds to the precession of the spins within the a-b plane and therefore can depend only on the in-plane anisotropy E. From Eq. (4b) it may be seen that $E_0(2)$ will also depend on the out-of-plane anisotropy D unless $\eta = \eta'$. We therefore conclude that in fact η must be taken equal to η' and we use $\eta = \eta' = (1 - 1/2S)$. We make this somewhat arbitrary choice mainly because we know that at least Eq. (3a) reproduces the single-ion ground state and first excited states correctly.

Inspection of Eqs. (3) and (4) shows that the difficulty in treating the out-of-plane anisotropy arises because $S_{z'}$ and $S_{x'}$, both of which are in-plane components in NiF_2, are approximated differently in (3), thus becoming inequivalent. This introduces some apparent out-of-plane energy into Eq. (4b). The x', y', and z' axes are defined below, after Eq. (7).

2. *Dispersion Relations*

The energy dispersion relations for NiF_2 have been given by Moriya,[17] although in his expressions η was taken equal to 1. Including the factor $\eta = (1 - 1/2S) = \frac{1}{2}$, we find that the energies of the two modes are given by

$$E_q(1) = [(a_q - d_q)^2 - (c_q + 2b_q)^2]^{1/2}$$

and (5)

$$E_q(2) = [(a_q + d_q)^2 - (c_q - 2b_q)^2]^{1/2} \quad ,$$

where

$$a_q = [(D - 3E\sin 2\delta)\eta + \gamma_{20}\cos 2\delta - \gamma_{10} - \gamma_{30} + \gamma_{1q} + \gamma_{3q}] \quad ,$$

$$b_q = \tfrac{1}{2}\eta(D + E\sin 2\delta) \quad , \tag{6}$$

$$c_q = \tfrac{1}{2}\gamma_{2q}(1 + \cos 2\delta) \quad ,$$

and

$$d_q = \tfrac{1}{2}\gamma_{2q}(1 - \cos 2\delta) \quad .$$

The canting angle δ is found to be

$$\delta = -\eta E / 8J_2$$

by setting the terms linear in the deviation operators equal to zero. γ_{lq} is the lth component of the Fourier transform of the exchange

$$\gamma_{lq} = \sum_{\delta_l} J_l e^{i\vec{q}\cdot\vec{\delta}_l} \quad ,$$

so that

$$\gamma_{1q} = 2J_1 \cos q_{y'}c \quad ,$$

$$\gamma_{2q} = 8J_2 \cos\tfrac{1}{2}q_{x'}a \cos\tfrac{1}{2}q_{z'}a \cos\tfrac{1}{2}q_{y'}c \quad , \tag{7}$$

and

$$\gamma_{3q} = 2J_3(\cos aq_{x'} + \cos aq_{z'}) \quad .$$

Here the axes are chosen so that $O_{x'}$ and $O_{z'}$ are in the a-b plane with z' along the crystal axis closest to the spin direction, and $O_{y'}$ is along the c axis of the crystal. From the symmetry of the γ_{lq} it can be seen that all domains have the same spin-wave spectrum.

The modes are split at $\vec{q} = 0$ due to the nature of the single-ion anisotropy, but become degenerate at the zone boundary in the approximation of the dipolar interactions we have used. The energies at the zone-boundary points, and at $\vec{q} = 0$, are listed in terms of the spin-Hamiltonian parameters in Table I. These points are referred to the crystal axes (X, Y, Z) parallel to (a, b, c). The $R(\frac{1}{2}, 0, \frac{1}{2})$ and $U(0, \frac{1}{2}, \frac{1}{2})$ points will be taken to be degenerate unless they are specifically distinguished; they differ in NiF_2 only due to the small canting of the spins. In writing Eq. (5) we have omitted the

TABLE I. Spin-wave energies at special points in the Brillouin zone in terms of the spin-Hamiltonian parameters. Small energies of the order of $E\delta$ have been ignored.

Point	q		E_{ZB}
Γ	$(0, 0, 0)$	(Mode 1)	$(32J_2\eta D + 4\eta^2E^2)^{1/2}$
Γ	$(0, 0, 0)$	(Mode 2)	$4\eta E$
X	$(\frac{1}{2}, 0, 0)$		$\eta D + 8J_2 - 4J_3$
Z	$(0, 0, \frac{1}{2})$		$\eta D + 8J_2 - 4J_1$
R, U	$(\frac{1}{2}, 0, \frac{1}{2})$		$\eta D + 8J_2 - 4J_1 - 4J_3$
M	$(\frac{1}{2}, \frac{1}{2}, 0)$		$\eta D + 8J_2 - 8J_3$
A	$(\frac{1}{2}, \frac{1}{2}, \frac{1}{2})$		$\eta D + 8J_2 - 4J_1 - 8J_3$

higher-order renormalization of the spin-wave energy. Using Oguchi's theory,[23] it amounts to essentially a constant correction of less than 4% over the entire zone.

IV. NEUTRON SCATTERING FROM NiF_2

A. Measurements

The neutron scattering measurements were made at 4.2 °K on a crystal of volume ~0.5 cc. The crystal was mounted with an [010] axis vertical so that values of $\vec{q}$ lay in the a-c plane.

Preliminary measurements were made on the Pluto time-of-flight spectrometer[24] at AERE Harwell, but all the data presented in this paper were taken at the H7 triple-axis spectrometer at the Brookhaven high-flux beam reactor using standard constant-Q techniques.

The use of pyrolytic graphite crystals, (002) planes, both as monochromator and analyzer enabled measurements to be made very quickly. Typical neutron groups giving points on the dispersion curve took between 10 and 30 min, although up to 2 h was spent on points such as at the zone boundary where high accuracy was required. Incident neutrons of 30 meV (~ 242 cm^{-1}) were used in order to avoid confusion by the effects of $\frac{1}{2}\lambda$ contamination present if lower energies were used. Because of the rather poor quality of the crystals, the value of $\vec{q}$ could not be determined with certainty to better than ~ 0.04 reciprocal-lattice units, and for this reason only careful measurements of the zone-boundary energy at the X, Z, and R points were used in the determination of the spin-Hamiltonian parameters. The dispersion was measured, however, in the three principal directions [001], [100], and [101] about the (100)M and (001)M reciprocal-lattice points. This provided a check on the parameters determined to within the accuracy of alignment.

The data are shown in Figs. 3(a)-3(c), and in Table II. In the [ζ 0 0] direction difficulty was experienced in obtaining the lower magnon energies, and at some points evidence for three excitations were observed. It is possible that the acoustic-phonon branch[25] lies close to the magnon branch in this direction over a range of $\vec{q}$, and affects the latter through interaction. However, further investigation of this point must await the availability of better crystals. Only the unambiguous magnon data is shown in Fig. 3(b).

Since the dispersion at the zone boundary is small, instrumental resolution corrections[26] are unnecessary. These may broaden the magnon line width observed, but will not shift the position of the peak intensity. In contrast, the observed $\vec{q}=0$

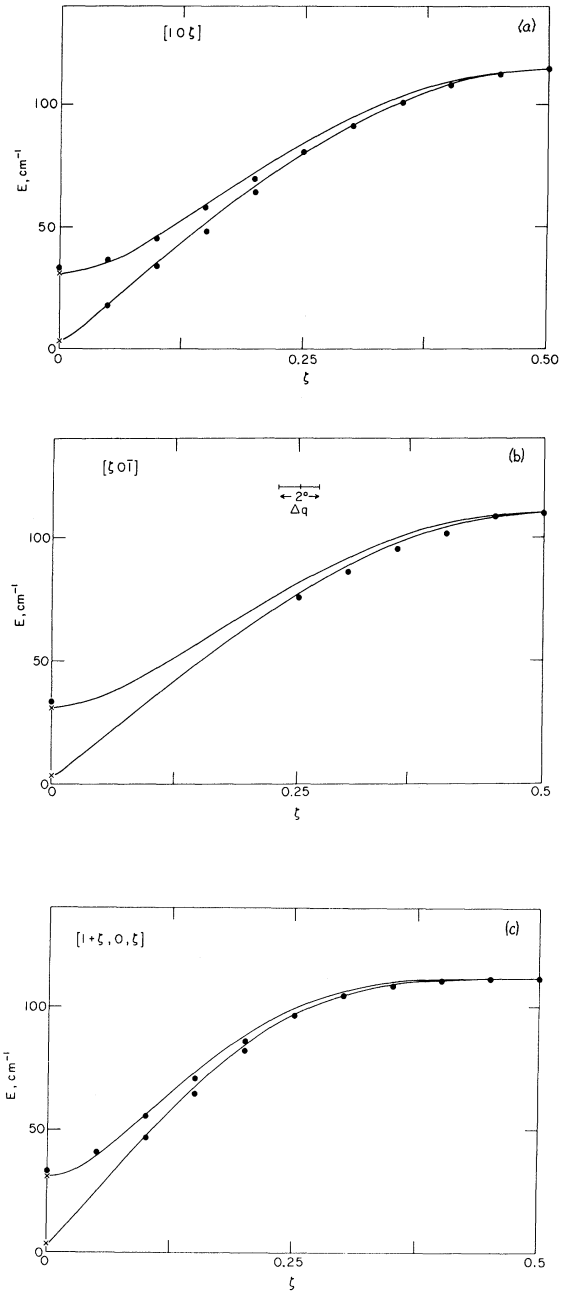

FIG. 3. (a) Magnon dispersion in the [00ζ] direction. ζ is in reciprocal-lattice units. The dots are the experimental points, crosses are Richards's antiferromagnetic-resonance frequencies, and the solid line is calculated from the parameters given in Table III. (b) Magnon dispersion in the [ζ00] direction. The symbols are as in Fig. 3(a). The range of possible error in q due to the mosaic spread of the crystal is indicated. Typical errors in energy of the measured points is ~1% for the higher energies, 3–4% for the lower energies. (c) Magnon dispersion in the [ζ0ζ] direction. The symbols are as in Fig. 3(a).

TABLE II. Measured and calculated zone-boundary energies in NiF_2. The calculated values use the parameters listed in Table III determined from the neutron and infrared data. Two-magnon energies ignoring magnon-magnon interactions are also given.

Point	q	Method	E_{ZB} (cm^{-1})	$2E_{ZB}$ (cm^{-1})
X	$(\frac{1}{2},0,0)$	Measured	110.02 ± 1.21	220.04 ± 2.4
Z	$(0,0,\frac{1}{2})$	Measured	114.05 ± 0.81	228.1 ± 1.6
R, U	$(\frac{1}{2},0,\frac{1}{2})$	Measured[a]	110.91 ± 0.81	221.8 ± 1.6
M	$(\frac{1}{2},\frac{1}{2},0)$	Calculated[a]	106.87 ± 0.40	213.8 ± 0.8
A	$(\frac{1}{2},\frac{1}{2},\frac{1}{2})$	Calculated	107.75 ± 2.40	215.6 ± 4.8

[a]Emphasized in Raman scattering.

excitations lie higher than the antiferromagnetic-resonance frequencies because of the effect of instrumental resolution and high dispersion in this region. The latter were used in the analysis because of their higher accuracy.

B. Analysis and Results

The three measured zone-boundary energies, at the X, Z, and R points, were used with the two $\vec{q}=0$ energies measured by Richards[10] to determine the five parameters in the Hamiltonian [Eq. (2)] from the expressions given in Table I. The values of the two anisotropy constants, and three exchange constants determined in this manner, are given in Table III.

We find that J_2 is the largest interaction, J_1 is small and probably ferromagnetic in sign, and J_3 is a little larger and antiferromagnetic. The anisotropy parameter D is close to the value found for Ni^{2+} in ZnF_2,[19] whereas that for E is somewhat smaller. Also given in Table III are the values for the parameters found from previous works. These mostly assume only one predominant exchange interaction. In addition, they generally are obtained from analyses of bulk magnetic measurements using either molecular field or first-order spin-wave theory, so that for $S=1$ they are expected to be accurate only to about 10%. The values given for the canting angle δ are calculated. In the present work we use Eq. (6). From the exchange constants we calculate an average Curie-Weiss $\bar{\theta}$ (paramagnetic Curie point) of $\bar{\theta}=109 \pm 7$ °K, and a value of $\theta_\perp$, corresponding to the perpendicular susceptibility of 108 ± 7 °K. These may be compared with the experimental values of $\bar{\theta}=144$ °K (Joenk and Bozorth[7]), and $\theta_\perp=128 \pm 10$ °K (Cooke *et al.*[8]). In view of the experimental difficulty of directly measuring a Curie-Weiss θ, the difference is probably not significant, particularly in light of the fact that neither determination of θ was made at very high T/θ values. The large value Joenk and Bozorth find for $\bar{\theta}$ also leads them to deduce $2J_1+4J_3=41 \pm 3$ °K, which is in clear disagreement with our value of $2J_1+4J_3=3.9 \pm 3.7$ °K.

The energy dispersion calculated from the values in the top line of Table III is shown as the full line in Figs. 3(a)–3(c), where it is seen that there is very reasonable agreement, in view of the experimental difficulty mentioned above. Calculated values of the spin-wave energy at the principal zone-boundary point not measured are given in Table II. It should perhaps be pointed out that these calculated values also depend for their accuracy on the validity of the three-exchange-parameter model. It is possible that more distant exchange interactions such as J_4 and J_5, which are highly correlated with

TABLE III. Values found for the Hamiltonian parameters [Eq. (2)] in cm^{-1}.

	E	D	J_1	J_2	J_3	δ
Present work	1.66 ± 0.03	4.36 ± 0.14	-0.22 ± 0.50	13.87 ± 0.36	0.79 ± 0.40	0.43 ± 0.02
Cooke *et al.* (Ref. 8.)	2.3 ± 0.2			13.4 ± 0.3		0.61 ± 0.08
Richards (Ref. 10)	1.66	3.86		15.63		0.38
Joenk and Bozorth (Ref. 7)	1.65 ± 0.03	3.1 ± 1.2		15.25		0.39
Ni^{2+} in ZnF_2 Peter and Mock (Ref. 19)	2.67	4.19				

the other parameters in the a-c plane, may affect these zone-boundary energies. However, the magnitude of these more distant exchange interactions is expected to be very small.

The density of magnon states may easily be calculated using a computer, and the result of stepping q over 10^6 points in the Brillouin zone and adding the number of points giving energies within ranges E and $E + 0.25\,\mathrm{cm}^{-1}$ is shown in Fig. 4. Both spin-wave branches were included equally in the summation. The density of states peaks sharply near $108\,\mathrm{cm}^{-1}$, the other singularities appearing as smooth shoulders on this peak. We shall utilize this feature of the density of states in discussing the two-magnon Raman-scattering line shape later.

V. LOW-TEMPERATURE LIGHT SCATTERING FROM NiF_2

A. Measurements

Details pertaining to the apparatus and techniques employed in the light scattering experiments were given previously by Fleury and Loudon.[27]

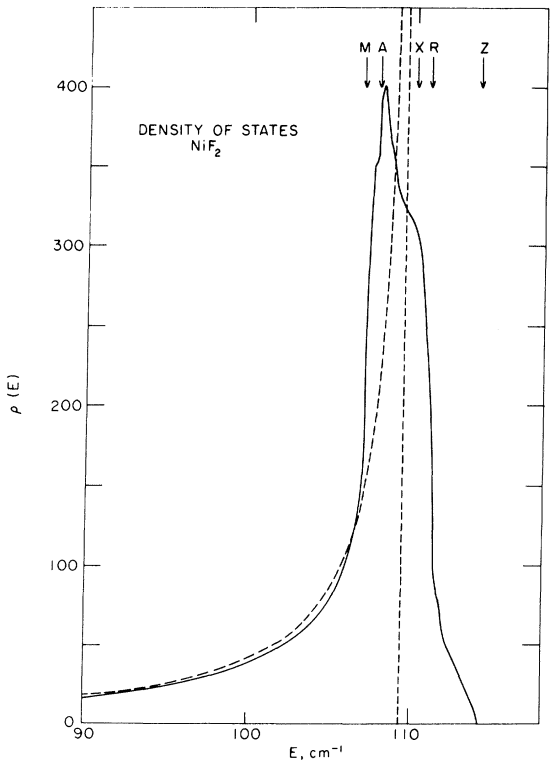

FIG. 4. Density of magnon states in NiF_2 calculated from the neutron data (solid line). The dashed line is the density of states for the one-exchange-parameter model used in the calculation of the Raman-scattering line shape.

The NiF_2 sample had the same mosaic spread $\sim 1-2^\circ$ as that used for the neutron experiments and, in fact, it was cut from the same boule. For most low-temperature runs, it was mounted in a glass Dewar and cooled by a stream of cold helium gas. Temperatures as low as 10 °K could be conveniently maintained with this scheme. In order to verify that there were no significant differences in the spectra at lower temperatures, some data were taken with the sample immersed in liquid helium, pumped to a temperature of ~1.8 °K.

The arrangement for the magnetic field experiments was also described by Fleury and Loudon.[27] The sample was mounted in the bore of a 50 kOe superconducting magnet, which was immersed in liquid helium. Because the sample was essentially on a "cold finger" (the bore wall) the temperature of the NiF_2 for the high-field experiments was in the vicinity of 20 °K.

In all of the experiments the geometry was such that any of the elements of the Raman tensor in the laboratory frame could be individually examined. Unfortunately, because of the inequivalence of the X and Y directions along the a and b axes in the antiferromagnetic phase of NiF_2, and because of the random distribution of "X" and "Y" domains below 73 °K, it is difficult to distinguish between certain elements of the Raman tensors for the magnetic scattering. Note that the coordinate system used here is rotated by 45° in the X-Y plane from that of some other authors,[6,10] and differs from that used in Eqs. (5) and (7) for the description of the magnon dispersion.

B. Results

1. *Phonons*

Although this paper is not directly concerned with the phonon properties of NiF_2, we shall briefly comment on the phonon Raman spectrum in order to help distinguish the magnon spectrum. Insofar as the phonons and magnons are uncoupled, NiF_2 can be considered to be of space group D_{4h}^{14}. Like other rutile-structure compounds, the four Raman-active modes[28] are of symmetries A_{1g}, B_{1g}, B_{2g}, and E_g. We have observed all four modes at temperatures between 1.8 and 300 °K with no anomalous changes in frequency or intensity over this range. In particular, because there is no change in the chemical unit cell at T_N, the phonon spectrum is unaffected by the antiferromagnetic phase transition. Figure 5 summarizes the phonon spectrum at ~ 80 °K. The frequencies are

$$A_{1g} = 410\ \mathrm{cm}^{-1},\quad B_{1g} = 70\ \mathrm{cm}^{-1},\quad B_{2g} = 536\ \mathrm{cm}^{-1},$$

and

$$E_g = 305\ \mathrm{cm}^{-1}.$$

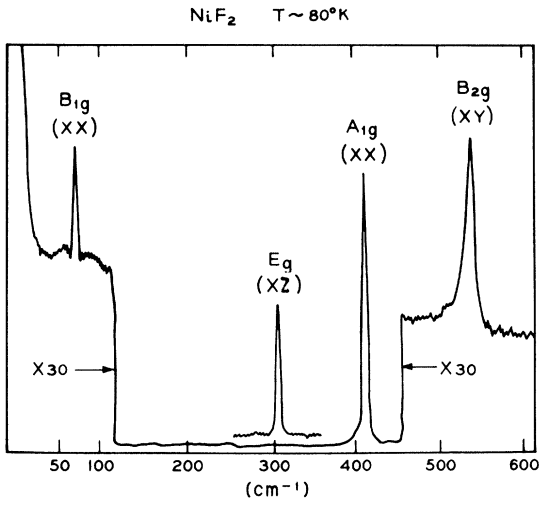

FIG. 5. Phonon-Raman spectrum of NiF_2. The sensitivity scale for the E_g and A_{1g} phonons is 30 times less than that for the B_{1g} and B_{1g} phonons.

The relative strengths of some selected Raman-tensor components are illustrated in Fig. 5. For further discussion of the phonons in the rutile-structure materials the reader is referred to Ref. 28. The most striking difference between the phonon and magnon spectra is the temperature dependence of the latter. In addition, the Raman tensor for one-magnon scattering is antisymmetric, and this fact may be used to distinguish it from phonon scattering. This point is discussed fully by Fleury and Loudon.

2. *One-Magnon Excitation*

The Raman spectrum of Fig. 6 illustrates scattering from the upper magnon mode, as well as from the two-magnon excitation at ~ 205 cm^{-1} to be discussed later. At ~ 10 °K the strength of the one-magnon scattering is about one-quarter that of the B_{1g} phonon, and about $\frac{1}{20}$ that of the two-magnon scattering. The xz and yz components of the one-magnon Raman tensor were observed to be equal and much larger than either the xy or xx components. The temperature dependence of the one-magnon frequency and linewidth agrees with the infrared (IR) results of Richards.[10]

Effects of magnetic field on the one-magnon line were less clear. First, the shift of the line was less than 1 cm^{-1} in fields of up to 50 kOe, applied either parallel or perpendicular to the c direction. This behavior also agrees with the IR results. However, on some runs certain elements of the one-magnon Raman tensor were observed to vanish as the field was increased above about 2 kOe. The amount of decrease for a given field varied from run to run. This suggests that the effects of magnetic domains are important here. Richards claims that a field of 5 kOe applied in the [100] direction is sufficient to align the domains. With all the domains aligned, X and Y directions in the laboratory become truly inequivalent, and rigorous one-magnon polarization selection rules should be observed. The field effects qualitatively agree with such an interpretation. The effects of strain on NiF_2 domain structure might then be invoked to explain the lack of quantitative reproductibility in successive experiments.

3. *Two-Magnon Excitations*

As has been shown earlier[27] magnon pairs scatter light most efficiently through an excited-state exchange mechanism, rather than the spin-orbit coupling responsible for one-magnon scattering. This difference in mechanism accounts for the initially surprising observation that second-order magnon Raman effect is more than an order of magnitude stronger than the first-order effect in NiF_2. As in the previously studied two-sublattice antiferromagnets FeF_2, MnF_2,[27] and $RbMnF_3$,[12] the two-magnon state excited in the light-scattering process is of positive parity and zero net spin. The magnon pair thus consists of one magnon from each of the two sublattices. The shape of the two-magnon spectrum is determined primarily by the joint magnon density of states, properly weighted according to the dictates of crystal symmetry. More recent work[11,12] has shown that the two-magnon line shape is significantly affected by magnon-magnon interactions as discussed in Sec. VI, and that the extended range parameter of the excited-state exchange is unnecessary. Symmetry requirements provide a connection between the polarization properties of the scattered light and the neighborhood of the Brillouin zone in which the individual magnon wave vectors terminate. A complete dis-

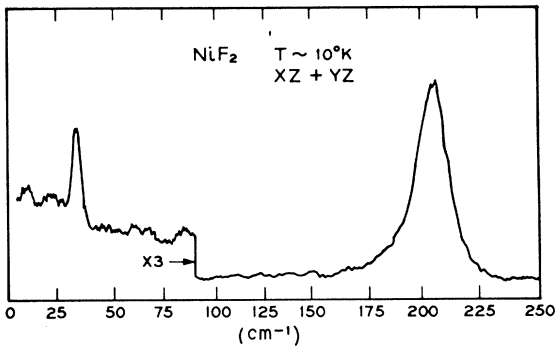

FIG. 6. Magnetic light scattering in NiF_2. The sharp peak at 31 cm^{-1} is due to a single zone-center magnon. The ~ 200-cm^{-1} peak is a magnon-pair excitation.

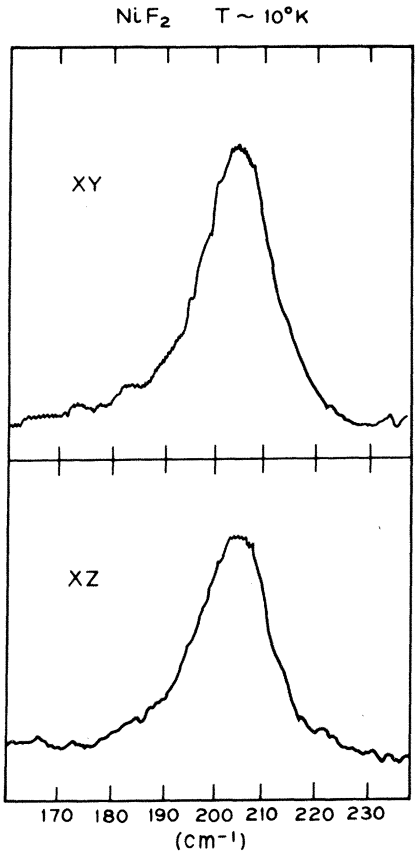

FIG. 7. The xz and xy Raman tensor contributions to the magnon pair scattering. As explained in the text, the similarity in shape and position of these peaks argues for near equality of magnon frequencies near the M, U, and R points of the NiF_2 Brillouin zone.

cussion of the theory for antiferromagnets such as MnF_2, with the moment directed along the c axis, was given earlier.[27] The same arguments applied to NiF_2 show that for "Y" domains the Raman-tensor elements α_{xx}, α_{yy}, α_{zz}, and α_{yz} receive dominant contributions from Γ- and R-point magnons, whereas α_{xy} and α_{xz} are dominated by M- and U-point magnons. For "X" domains the subscripts x and y should be interchanged. Assuming a random distribution of X and Y domains within the scattering volume, the experimentally observed α_{xz} should receive equal contributions from R-point and M- and U-point magnons, whereas α_{xy} should depend on M- and U-point magnons alone. As shown in Fig. 7, there is no discernable difference between α_{xy} and α_{xz} in the laboratory frame. This observation implies that the frequencies of M- and R- and U-point magnons in NiF_2 are very nearly equal, and permits one to combine α_{yx} and α_{yz} (as in Fig. 8) to obtain better signal to noise and higher resolution for comparison with theory.

The two-magnon Raman-tensor elements for nearly strain-free regions of the crystal are observed to be $\alpha_{xz} \approx \alpha_{yz} \approx \alpha_{xy}$. These off-diagonal terms are larger than the diagonal elements α_{xx}, α_{yy}, and α_{zz} by an order of magnitude.

The scattering efficiencies of one- and two-magnon excitations in NiF_2 are comparable to those observed in other transition metal fluorides.[27] In particular, the extinction coefficient (defined as the fraction of light scattered per unit path length per unit solid angle) for the magnon-pair excitation in NiF_2 is $\sim 10^{-11}$ cm^{-1} sr^{-1}, approximately three times greater than the corresponding quantity in FeF_2. However, the one-magnon scattering in NiF_2 is about three times weaker than in FeF_2.

Magnetic field experiments, under conditions described above, revealed no discernable effect on the two-magnon scattering for $\vec{B}$ either parallel or perpendicular to the c direction. Although two-magnon absorption of IR[29] radiation is expected in NiF_2, the presence of a strong absorption due to the E_{1u} phonon[30] at 227 cm^{-1} has prevented its observation.

From the neutron scattering results and the theoretical analysis in Sec. VI, we shall see that the effects of magnon-magnon interactions are quite evident in the low-temperature two-magnon Raman spectra of NiF_2.

VI. THEORY OF RAMAN SPECTRA MAGNON-MAGNON INTERACTIONS

It has been shown[11,31] previously that two-magnon

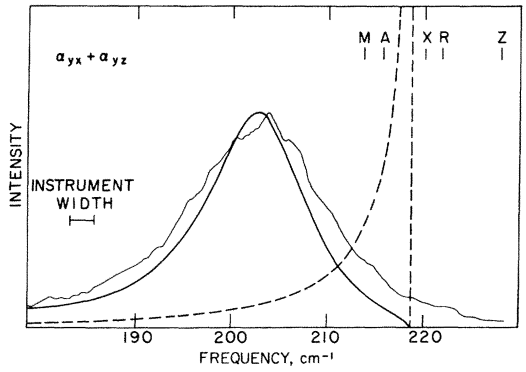

FIG. 8. The experimental line shape for the Raman scattering ($\alpha_{yx} + \alpha_{yz}$) is compared with theory using a single exchange parameter $J = 13.68$ cm^{-1}. The theory without interactions included is shown by a dotted line and the theory with magnon-magnon interactions is the solid line. The only adjustable parameter is the peak height which is chosen to coincide with experiment. The instrumental width in the experimental spectrum is ~ 2.5 cm^{-1}.

optical experiments can only be understood satisfactorily if the interaction between the two magnons is included. The reason that the interaction is so important is clear. The photon creates spin deviations on neighboring sites where they interact strongly. The two-spin deviations can be thought of as wave packets of magnons which propagate through the lattice but are initially in close proximity.

The original work[11,12,31] on $RbMnF_3$ produced excellent agreement between theory and experiment. This was possible because the magnons in $RbMnF_3$ can be described by a single exchange constant and so the density of states has a single peak. Recent work[13] on MnF_2 has shown that exchange between more distant neighbors introduces more structure into the density of states which complicates the situation considerably as the various two-magnon modes are associated with different peaks in the density of states.[32] It is therefore essential to include at least two exchange constants to describe the magnon dispersion curves, and the interaction effects, in order to understand the two-magnon spectra of MnF_2.[13]

We have seen from Sec. IV that the exchange in NiF_2 is predominantly next nearest neighbor but there are small (~5%) exchange interactions between other neighbors. These are much smaller than in MnF_2, and from Fig. 4 we see they are *not* large enough to give two distinct peaks in the density of states. We therefore feel confident in using a model involving only one exchange constant to interpret the Raman scattering in NiF_2. We chose the single exchange parameter, $J_2 = 13.68$ cm^{-1}, to give a magnon band from 0 to 109.4 cm^{-1} (the weighted-average zone-boundary energy). The neglect of crystal field effects that produce canting and finite antiferromagnetic-resonance frequencies is not serious since the two-magnon Raman experiments only probe magnons on or near the zone boundary. The density of states for such a model is also shown in Fig. 4.

The theory now becomes identical to that described for CoF_2 in a previous paper[31] (except that the anisotropy is put equal to zero and the spin is 1). The scattered intensity $I(\omega)$ for the d mode (visible in either xy, yz, or zx polarizations) is given by

$$I(\omega) \propto \mathrm{Im}\left(\frac{\mathcal{G}(\omega)}{1+(4Sz-1)J_2^2\,\mathcal{G}(\omega)}\right) , \tag{8}$$

where

$$\mathcal{G}(\omega) = \frac{1}{N}\sum_{\vec{q}} \frac{8\sin^2\tfrac{1}{2}q_x a \sin^2\tfrac{1}{2}q_y a \cos^2\tfrac{1}{2}q_z c}{\omega^2 - 4\omega_{\vec{q}}^2} , \tag{9}$$

$$\omega_{\vec{q}} = SzJ_2(1-\cos^2\tfrac{1}{2}q_x a \cos^2\tfrac{1}{2}q_y a \cos^2\tfrac{1}{2}q_z c)^{1/2} . \tag{10}$$

We use here the coordinate system of Sec. V, and the parameters in the above expressions are $S = 1$, $z = 8$, and $J_2 = 13.68$ cm^{-1}. Expressions (8) and (9) are actually for the xy polarization. However, because $\mathcal{G}(\omega)$ does not depend on the ratio c/a, identical expressions are obtained for the yz and zx polarizations (i.e., the crystal becomes effectively cubic). Inclusion of next-neighbor exchange would mean that $\alpha_{xy} \neq \alpha_{yz}$. Experimentally $\alpha_{xy} \approx \alpha_{yz} \approx \alpha_{zx}$, so that we see that next-neighbor exchange is not visible in the Raman spectra. The other Raman mode with elements α_{xx}, α_{yy}, and α_{zz} has small intensity as expected for an s mode.[31]

The calculated intensity is compared with experiment in Fig. 8. The theory and experiment agree extremely well and would agree even better if the instrumental width were deconvoluted from the experimental results. The scattered intensity without the magnon-magnon interaction is shown as a dotted line [$\propto \mathrm{Im}\,\mathcal{G}(\omega)$]. The large effect of the magnon-magnon interaction is apparent, the line center being shifted from 219.8 to 202.7 cm^{-1} and the width increased considerably.

VII. DISCUSSION

The values of the exchange constants may be compared with those found in other rutile compounds. These are listed, together with the present results, in Table IV. It can be seen that in all the compounds listed except VF_2 the corner to body-center interaction J_2 is largest and predominates. J_1, linking ions along the c axis, is ferromagnetic, and J_3 is small and antiferromagnetic. The magnetic structure of VF_2[33] requires $J_1 > 10J_2$[34] and thus the predominant interaction changes dramatically in these compounds. The series should provide a good test for theories of superexchange.

The fact that the Raman spectra can be well explained in terms of the neutron results and magnon-magnon interaction lends further support to the proposition that the factors affecting the two-magnon optical spectra are now well understood. The combined results from both one- and two-magnon light scattering can thus provide quantitative values for the dominant exchange and anisotropy for antiferromagnets. The results show that the theory holds well for an $S = 1$ ion, and for the case of a canted antiferromagnet. They suggest that a simple one-parameter model may be applied with success in case where the magnon density of states shows a predominant peak as its main feature. Although no theory has yet been worked out for the magnon interaction effects at elevated temperatures, the two-magnon Raman spectrum of NiF_2 has been followed experimentally to temperatures

TABLE IV. Comparison of effective anisotropy and exchange constants in cm^{-1} in rutile flourides.

	T_N(°K)	Magnetic structure[a]	Spin or effective spin[+]	Effective anisotropy energy ($g\mu_B H_A$)	J_1	J_2	J_3
VF_2 (Ref. 33)	7.0	a	$\frac{3}{2}$	...	$J_1 > 10J_2$		...
MnF_2 [b]	67.4	b	$\frac{5}{2}$	0.74	−0.44	2.45	<0.06
FeF_2 (Ref. 14)	78.4	b	2	20.1	−0.05	3.64	0.19
CoF_2 [c]	37.7	b	$\frac{3}{2}$+	...	−0.83	4.54	...
NiF_2 [d]	73.2	c	1	...	−0.22	13.87	0.79

[a]Structures: a, spiral along c axis, spins in a-b plane; b, type 1 body-centered tetragonal, spins parallel to c axis; c, type 1 body-centered tetragonal, spins canted in a-b plane.

[b]A. Okazaki, K. C. Turberfield, and R. W. H. Stevenson, Phys. Letters 8, 9 (1964).

[c]Values quoted by E. Belorizky, S. C. Ng, and T. G. Phillips, Phys. Rev. 181, 467 (1969), as private communication from R. A. Cowley.

[d]This work.

well above $T_N = 73$ °K.[35] The fact that light scattering samples a portion of the four-spin correlation function, whereas neutron scattering probes the two-spin correlation function, suggests that neutron experiments in NiF_2 at higher temperatures would provide valuable information for the development of a theory of magnon interactions at higher temperatures.

VIII. SUMMARY

In this paper we have reported the investigation of magnons in NiF_2 at low temperatures by inelastic neutron and Raman light scattering. The neutron data have been analyzed to give values of the parameters describing the exchange and anisotropy in the crystal Hamiltonian. The density of magnon states calculated from these parameters shows one sharp peak as its main feature. Two-magnon scattering of light with different polarizations confirms that the zone-boundary energies of the magnons lie close to each other. By adopting a simple model in which the weighted-average zone-boundary energy is used to define a single effective exchange constant descriptive of the density of states, the Raman line shape and frequency can be explained very well by a Green's-function theory of magnon-magnon interactions in a cubic antiferromagnet.

*Work supported by the U. S. Atomic Energy Commission.

†Guest scientist at Brookhaven National Laboratory, Upton, N. Y. 11973.

[1]J. W. Stout and S. A. Reed, J. Am. Chem. Soc. 76, 5279 (1954).

[2]J. W. Stout and E. Catalano, J. Chem. Phys. 23, 2013 (1955).

[3]R. A. Alikanov, Zh. Eksperim. i Teor. Fiz. 37, 1145 (1959) [Soviet Phys. JETP 10, 814 (1960)].

[4]R. G. Shulman, Phys. Rev. 121, 125 (1961).

[5]L. M. Matarresse and J. W. Stout, Phys. Rev. 94, 1792 (1954).

[6]T. Moriya, Phys. Rev. 117, 635 (1960).

[7]R. J. Joenk and R. M. Bozorth, in *Proceedings of the International Conference on Magnetism, Nottingham*, 1964 (the Institute of Physics and the Physical Society, London, 1965), p. 493.

[8]A. H. Cooke, K. A. Gehring, and R. Lazenby, Proc. Phys. Soc. (London) 85, 967 (1965); 86 1377 (1965).

[9]P. L. Richards, J. Appl. Phys. 35, 850 (1964).

[10]P. L. Richards, Phys. Rev. 138, A1769 (1965).

[11]R. J. Elliott, M. F. Thorpe, G. F. Imbusch, R. Loudon, and J. B. Parkinson, Phys. Rev. Letters 21, 147 (1968).

[12]P. A. Fleury, Phys. Rev. Letters 21, 151 (1968).

[13]M. F. Thorpe, J. Appl. Phys. 41, 892 (1970).

[14]M. T. Hutchings, B. D. Rainford, and H. J. Guggenheim, J. Phys. C 3, 307 (1970).

[15]Although recently two-magnon Raman scattering has been reported in the perovskite $KNiF_3$, where it is found that theory including magnon-magnon interaction effects gives a good account of the line shape. See S. R. Chinn, H. J. Zeiger, and J. R. O'Connor, J. Appl. Phys. 41, 894 (1970).

[16]K. Haefner, J. W. Stout, and C. S. Barrett, J. Appl. Phys. 37, 449 (1966).

[17]T. Moriya, J. Phys. Soc. Japan 21, 926 (1966).

[18]S. J. Joshua and A. P. Cracknell, J. Phys. C 2, 24 (1969).

[19]M. Peter and J. B. Mock, Phys. Rev. 118, 137 (1960).

[20]G. F. Herrmann, J. Phys. Chem. Solids 24, 597 (1963).

[21]H. J. Fink, Phys. Rev. 133, A1322 (1964).

[22]L. R. Walker, in *Magnetism*, edited by G. T. Rado and H. Suhl (Academic, New York, 1963), Vol. 1, p. 299.

[23]T. Oguchi, Phys. Rev. 117, 117 (1960).

[24]R. F. Dyer and G. G. Low, in *Inelastic Scatterings*

of Neutrons in Liquids and Solids (International Atomic Energy Agency, Vienna, 1961), p. 179.

[25]Acoustic-phonons dispersion in rutile compounds has been measured by P. Martel, R. A. Cowley, and R. W. H. Stevenson, Can. J. Phys. 46, 1355 (1968); P. Kahn, J. P. Trotin, D. Cribier, and C. Beroit, in *Inelastic Scatterings of Neutrons in Liquids and Solids* (International Atomic Energy Agency, Vienna, 1969), p. 289.

[26]See, for example, M. J. Cooper and R. Nathans, Acta Cryst. 23, 357 (1967).

[27]P. A. Fleury and R. Loudon, Phys. Rev. 166, 514 (1968).

[28]S. P. S. Porto, P. A. Fleury, and T. C. Damen, Phys. Rev. 154, 522 (1967).

[29]P. L. Richards, J. Appl. Phys. 38, 1500 (1967).

[30]M. Balkanski, P. Moch, and G. Parisot, J. Chem. Phys. 44, 940 (1966).

[31]R. J. Elliott and M. F. Thorpe, J. Phys. C 2, 1630 (1969); M. F. Thorpe and R. J. Elliott, in *Light Scattering Spectra of Solids* (Springer-Verlag, New York, 1969).

[32]R. Loudon, Advan. Phys. 17, 243 (1968).

[33]M. T. Hutchings (unpublished); H. Y. Lau, J. W. Stout, W. C. Koehler, and H. R. Child, J. Appl. Phys. 40, 1136 (1969).

[34]A. Yoshimori, J. Phys. Soc. Japan 14, 807 (1959).

[35]P. A. Fleury, Phys. Rev. 180, 591 (1969). Similar experimental results on the temperature dependence of magnon-pair modes have been reported for $RbMnF_3$ and FeF_2 by P. A. Fleury, J. Appl. Phys. 41, 886 (1970).

PHYSICAL REVIEW B VOLUME 2, NUMBER 5 1 SEPTEMBER 1970

Path Integral Theory of Magnetic Alloys

D. R. Hamann

Bell Telephone Laboratories, Murray Hill, New Jersey 07974

(Received 1 April 1970)

The theory of dilute magnetic alloys is studied using Anderson's model. The Coulomb interaction is represented by the fluctuating potential acting on single electrons at the impurity site, and the partition function is rigorously formulated as a path integral over all possible time histories of this potential. For any particular path, the response of the electron gas is calculated using a method introduced by Nozières and De Dominicis, which is exact in the limit that the potential fluctuations are slow. From this, the contribution of any particular path to the partition function is obtained as an explicit and rather simple functional. When the Coulomb interaction is large compared to the width of the virtual bound state, a particular group of paths are singled out on the basis that they make the largest contributions. The functional is evaluated for this set of paths, and gives an expression which can be interpreted as the grand partition function for a one-dimensional gas of classical particles interacting through a logarithmic pair potential. This is identical to the result of a recent study of the $s-d$ exchange model by Anderson and Yuval. An analysis of this result has been given earlier, and it yields a satisfactory description of the Kondo effect. The resistivity is estimated, and found to approach the unitarity limit below the Kondo temperature and the Hartree-Fock value above the Kondo temperature. The correspondence between the Anderson and $s-d$ exchange models is shown to break down when the former is only weakly magnetic.

I. INTRODUCTION

This paper describes a new approach to the theory of dilute magnetic alloys.[1] The approach employs the Anderson model,[2] and bases its only approximations on a single widely held assumption: Spin polarization on the impurity persists much longer than it would in the absence of the Coulomb interaction. The goal of the investigation is to make firmly based predictions about the behavior of dilute alloys below the Kondo temperature, where perturbation expansions diverge.[3] Because the physical mechanism of the Kondo effect is not well understood, it is very difficult to give *a priori* justification to any approximation procedure. For this reason we have avoided the standard gambits of modern many-body theory, such as partial summation of perturbation expansions and decoupling equations of motion. While such schemes have the ability to continue the leading terms in high-temperature expansions to low temperatures, this ability is not a genuine criterion for their quality as low-temperature approximations. The key approximation in this study is purely mathematical; no class of diagram or type of correlation is excluded. Furthermore, the validity of the approximation can be established self-consistently from the behavior of the solution.